

Effects of a deformation of a star on the gravitational lensing

H. Asada^{*}

*GRACO, Institute for Astrophysics at Paris, 98bis boulevard Arago, 75014 Paris, France
Faculty of Science and Technology, Hirosaki University, Hirosaki 036-8561, Japan*

Accepted Received

ABSTRACT

We study analytically a gravitational lens due to a deformed star, which is modeled by using a monopole and a quadrupole moment. Positions of the images are discussed for a source on the principal axis. We present explicit expressions for the lens equation for this gravitational lens as a single real tenth-order algebraic equation. Furthermore, we compute an expression for the caustics as a discriminant for the polynomial. Another simple parametric representation of the caustics is also presented in a more tractable form. A simple expression for the critical curves is obtained to clarify a topological feature of the critical curves; the curves are simply connected if and only if the distortion is sufficiently large.

Key words: gravitational lensing – stars: general

1 INTRODUCTION

Some recent highly accurate numerical simulations of rotating compact objects such as a neutron star elucidate many features of compact objects such as an equilibrium configuration and its stability (e.g., Shibata et al. 2002, Stergioulas et al. 2004, Zanotti and Rezzolla 2002, Zdunik et al. 2004). The deformation of their configurations causes a non-spherical distortion of the surrounding spacetime, which has not been observed yet. Probing this warp of the spacetime provides a strong verification of the theory of the general relativity (Will 1993) and a deep insight into the relevant physics especially about the nuclear matter (e.g., Shapiro and Teukolsky 1983), because the deformation depends not only on the gravity but also on the equation of state of the internal matter.

One possibility is to study effects of the deformation on the light propagation near the compact object. Before doing numerical studies in detail, it is important to find some physical properties by using a simple analytic model. One reason is that one needs many light ray tracings in numerical investigations, and consequently it is difficult to clarify quantitatively the parameter dependence.

We perform the multipole expansion of the external gravitational field, which can be assumed to be weak along the line of sight even if the internal gravity is strong. Namely, one can consider only the linearized potential. This does not mean that our system is linear, because the lens equation is

non-linearly coupled with respect to the image positions as shown in the next section.

The quadrupole moment depends on the rotation speed and the equation of the state for the internal matter. Many years ago some comprehensive studies had been done for equilibrium configurations of rotating stars in the Newtonian gravity, some of which are summarized in a famous textbook (Chandrasekhar 1987). Numerical investigations on this issue in the general relativity are still going on as mentioned in the beginning of this section (e.g., Shibata et al. 2002, Stergioulas et al. 2004, Zanotti and Rezzolla 2002, Zdunik et al. 2004). In an extreme case called as rapid rotation, the quadrupole deviation of order of 10^{-3} may be possible even for a neutron star. These results show that the deformation is dominated by the quadrupole moment and higher moments such as the octapole moment are much smaller. In addition, a contribution of the octapole moment in the external field decays faster than that of the quadrupole moment, because the ratio between the octapole potential and the quadrupole potential is of the order of the ratio of the stellar radius to the distance between the star and the field point, which becomes the impact parameter in the gravitational lensing. This ratio is so small that one can ignore approximately the octapole and higher moment in the lensing study. Furthermore, radio observations such as the VLBI will be improved. If the accuracy is improved sufficiently, the present result will have a direct relevance with such an observation. Hence, we consider in this paper the truncated multipole expansion up to the quadrupole moment.

This consideration in the gravitational lens is not new but rather classical though it was done in a different context.

^{*} Email: asada@phys.hirosaki-u.ac.jp

For instance, the light deflection caused by the quadrupole moment of the Sun was discussed in the context of tests of the general relativity (Epstein and Shapiro 1980). Except for a case of the source on the equatorial plane, we need solve the lens equation numerically. A spherically symmetric galaxy and a quadrupole tidal part were extensively studied by Kovner (1987), in which most models are an extended sphere and the quadrupole part, and another model is a star with quadrupole shear induced by a galaxy where the star is located. The last model seems similar to our system of a deformed star. However, it should be noted that this extra shear does not come from a potential of the star but from that of the galaxy. In other words, the dependence of the shear on the radial coordinate is different from that for the deformed star.

It is believed that gravitational lensing study needs some numerical techniques except for a few special cases such as a point mass lens or an axisymmetric mass distribution along the line of sight, because the lens equation is nonlinearly coupled (for instance, Schneider et al. 1992). In recent, however, some development has been achieved: It has been shown that for two cases of a binary lens (Asada 2002) and an ellipsoidal lens (Asada et al. 2003) the lens equation is reduced to a single polynomial. An advantage of this approach is saving time and computer resources, and another one is to enable us to study analytically the lensing, for instance to find out an analytic expression for caustics (Asada et al. 2002, 2003) which are curves on the source plane, and the number of images changes if a source crosses the caustics. This expression for the caustics is nothing but a discriminant for the polynomial, which determines a change in the number of roots for the equation: As known in algebra, the discriminant vanishes in a case of multiple roots, which corresponds to merging images or giant arcs in the gravitational lens. Classification of the critical curves and caustics is of great importance. For instance, it was done intensively for a binary gravitational lens (e.g., Dominik 1999).

Furthermore, it has been shown also that one can derive a single polynomial equation for any set of the lens equations in polynomials by using the Euclidean algorithm (Asada et al. 2004). In practice, however, in a case of the lens equation which is higher than fifth degree, this algebraic procedure needs a computer with a fast CPU and a huge memory, and furthermore the resultant equation may become too complicated to handle any more in the Cartesian coordinates. In order to avoid this problem, the polar coordinates are adopted in this paper so that a simple result can be obtained.

This paper is organised as follows. First, we show that the lens equation is reduced to a single polynomial equation. Next, the analytic expression for the caustics is computed as the discriminant for the polynomial. Finally, a parametric representation for the critical curves and caustics are obtained to clarify a topological feature of the critical curves.

2 LENS EQUATION FOR A LENS WITH QUADRUPOLE MOMENT

2.1 Lens Equation

The lens equation relates the image angular position vector θ to the source angular position vector β as

$$\beta = \theta - \frac{D_{\text{LS}}}{D_{\text{S}}} \alpha(\xi), \quad (1)$$

where we used the thin-lens approximation, D_{S} is the angular distance from the observer to the source, and D_{LS} is that from the lens to the source. The vector ξ , which denotes the impact parameter to the light ray, is related to the image position as $\xi = D_{\text{L}} \theta$, where D_{L} is the angular distance from the observer to the lens.

Up to quadrupole moments in multipole expansions, the deflection angle $\alpha = (\alpha^1, \alpha^2)$ is given by

$$\alpha^i = \frac{4GM}{c^2} \frac{\xi^i}{|\xi|^2} + \frac{8G}{c^2} \left(\sum_{j,k=1}^2 2Q_{jk} \frac{\xi^j \xi^k \xi^i}{|\xi|^6} - \sum_{j=1}^2 Q_{ij} \frac{\xi^j}{|\xi|^4} \right). \quad (2)$$

Here M denotes the mass of the lens, and the quadrupole moment tracefree on the lens plane is defined as

$$Q_{ij} = \int \rho (X_i X_j - \frac{1}{2} \delta_{ij} |\mathbf{X}|^2) d^3 X, \quad (3)$$

where ρ denotes the mass density. It is worthwhile to mention that there are no contributions from quadrupole moment whose components are along the line of sight (Asada and Kasai 2000).

Now, a renormalisation is done in units of the Einstein ring angular radius defined as (for instance, Schneider et al. 1992)

$$\theta_{\text{E}} = \sqrt{\frac{4GM D_{\text{LS}}}{c^2 D_{\text{L}} D_{\text{S}}}}, \quad (4)$$

so that the lens equation is simply rewritten as

$$\tilde{\beta} = \tilde{\theta} - \tilde{\alpha}, \quad (5)$$

where $\tilde{\beta} = \beta/\theta_{\text{E}}$, $\tilde{\theta} = \theta/\theta_{\text{E}}$, and

$$\tilde{\alpha}^i = \frac{\tilde{\theta}^i}{|\tilde{\theta}|^2} + 2 \sum_{j,k=1}^2 \tilde{Q}_{jk} \frac{\tilde{\theta}^j \tilde{\theta}^k \tilde{\theta}^i}{|\tilde{\theta}|^6} - \sum_{j=1}^2 \tilde{Q}_{ij} \frac{\tilde{\theta}^j}{|\tilde{\theta}|^4}. \quad (6)$$

Here, the renormalised quadrupole moment is defined as

$$\tilde{Q}_{ij} = \frac{c^2 D_{\text{S}} Q_{ij}}{2GM^2 D_{\text{L}} D_{\text{LS}}}. \quad (7)$$

Eq. (5) is a set of coupled equations which are seventh-order in $\tilde{\theta}^1$ and $\tilde{\theta}^2$, respectively. It is apparent that we can hardly treat it analytically.

Before examining Eq. (5) in detail, we estimate the order of magnitude of the renormalised quadrupole moment. We can put $|\tilde{Q}_{ij}| \sim \varepsilon MR^2$, where ε denotes a distortion parameter and R is a typical size of the lens object. Truncations up to quadrupole moment in multipole expansions are valid if the asymmetry of the system is sufficiently small, say $\varepsilon < 1/10$, though we don't perform any expansion in ε . The renormalised quadrupole moment is rewritten as

$$|\tilde{Q}_{ij}| \sim 2\varepsilon \left(\frac{R}{R_{\text{E}}} \right)^2, \quad (8)$$

where $R_{\text{E}} = D_{\text{L}} \theta_{\text{E}}$ is the Einstein ring radius. In most cases, R is shorter than R_{E} . Thus, $|\tilde{Q}_{ij}|$ must be less than 2ε , which is usually $1/5$ at most.

For instance, we assume a nearby solar-type star at 10pc, namely $R_{\text{E}} \sim 10^7 \text{km}$, $R \sim 10^6 \text{km}$. If it rotates much faster than the Sun, say with the rotational surface velocity

on the equatorial plane $v \sim 10\text{km/s}$, the oblateness due to the centrifugal flattening is of the order of

$$\varepsilon \sim 10^{-3} \left(\frac{M_\odot}{M} \right) \left(\frac{R}{10^6\text{km}} \right) \left(\frac{v}{10\text{km/s}} \right)^2. \quad (9)$$

Then, \tilde{Q}_{ij} becomes about 10^{-5} . If a light ray passes near the surface of the star, the leading term of the deflection angle is about 1 arcsec. and the correction due to the quadrupole moment can be as large as 10 microarcsec., which will be detectable in principle by a near future astrometry mission such as GAIA and SIM, though such a probability may be extremely small.

Henceforth, we adopt a frame in which the reduced quadrupole moment is diagonalised as

$$\tilde{Q}_{ij} = \begin{pmatrix} e & 0 \\ 0 & -e \end{pmatrix}. \quad (10)$$

Without loss of generality, we can assume $e > 0$. By denoting $\tilde{\beta} = (a, b)$ and $\theta = (x, y) = (r \cos \phi, r \sin \phi)$ for $r \geq 0$, it is convenient to rewrite Eqs. (5) and (6) into a matrix form

$$\begin{pmatrix} a \\ b \end{pmatrix} = \begin{pmatrix} \cos \phi & \cos 3\phi \\ \sin \phi & \sin 3\phi \end{pmatrix} \begin{pmatrix} f \\ g \end{pmatrix}, \quad (11)$$

where

$$f = r - \frac{1}{r}, \quad (12)$$

$$g = -\frac{e}{r^3}. \quad (13)$$

Here, f and g depend on the mass and quadrupole moment, respectively, where we should remember that our renormalisation was done in units of the Einstein ring radius so that the mass does not appear explicitly.

2.2 Sources on the symmetry axes

First of all, we consider a source located at the origin $(a, b) = (0, 0)$, namely exactly behind the lens object. For $b = 0$, the second line of Eq. (11) means (1) $\sin \phi = 0$ or (2) $f + g(3 - 4 \sin^2 \phi) = 0$. The case (1) means $y = 0$, consequently $r^2 = x^2$. Then, the first line of Eq. (11) becomes

$$x^4 - x^2 - e = 0, \quad (14)$$

where we used $r \neq 0$. This equation is solved immediately as

$$x = \pm \sqrt{\frac{1 + \sqrt{1 + 4e}}{2}}, \quad (15)$$

where we used $\sqrt{1 + 4e} > 1$. Next, we consider the case (2), whose condition is rewritten as

$$f + 4g \cos^2 \phi = g. \quad (16)$$

By substituting this into the first line of Eq. (11), we obtain $g \cos \phi = 0$. Because of $g \neq 0$, we find $\cos \phi = 0$, which means $x = 0$ and $r^2 = y^2$. Then, Eq. (16) becomes simply $f = g$, which is rewritten as $y^4 - y^2 + e = 0$. This is solved as

$$y = \pm \sqrt{\frac{1 \pm \sqrt{1 - 4e}}{2}}, \quad (17)$$

which are real if and only if $e \leq 1/4$. Hence, we find two images given by Eq. (15) on x -axis, and four images by Eq. (17) on y -axis if $e \leq 1/4$, or otherwise only the first two images on x -axis.

Now, let us consider a case that a source is located on a symmetry axis but off the origin. For simplicity, we assume $b = 0$ and $a \neq 0$. The case of $a = 0$ and $b \neq 0$ is obtained simply by transforming $e \rightarrow -e$ and $x \leftrightarrow y$ as discussed later. For $b = 0$, the second line of Eq. (11) means (a) $\sin \phi = 0$ or (b) $f + g(3 - 4 \sin^2 \phi) = 0$. The case (a) means $y = 0$ and $r^2 = x^2$. Then, the first line of Eq. (11) becomes

$$u(x) \equiv x^4 - ax^3 - x^2 - e = 0, \quad (18)$$

where we used $r \neq 0$. The discriminant for this fourth-order polynomial (van der Waerden 1966) is computed as

$$D_4 = -e(16 + 128e + 256e^2 + 4a^2 + 144a^2e + 27a^4e), \quad (19)$$

which is negative. This implies that Eq. (18) has only two real roots. Furthermore, we find $u(0) = -e < 0$. The corresponding two images are located on x -axis, one positive and one negative each.

The case of $a = 0$ and $b \neq 0$ is more complicated. The transformation mentioned above gives us

$$v(y) \equiv y^4 - by^3 - y^2 + e = 0, \quad (20)$$

which is the second line of Eq. (11). For this equation, the discriminant becomes

$$D_4 = e(16 - 128e + 256e^2 + 4b^2 - 144b^2e - 27b^4e). \quad (21)$$

$D_4 = 0$ has two roots

$$b^2 = b_\pm^2, \quad (22)$$

where we defined

$$b_\pm^2 = \frac{2}{3^3e} [(1 - 2^2 3^2 e) \pm (1 + 2^2 3e)^{3/2}]. \quad (23)$$

One can show that $b_-^2 < 0$ and $b_+^2 > 0$. Hence, for $b^2 > b_+^2$, we find $D_4 < 0$, which implies two real roots, namely two on-axis images. On the other hand, for $b^2 < b_+^2$, we find $D_4 > 0$, which implies either four or no real roots. Further investigations are thus needed. We use the derivative of $v(y)$ as

$$v'(y) = y(4y^2 - 3by - 2). \quad (24)$$

The solutions of $v'(y) = 0$ are $y = 0, y_\pm$, where we defined

$$y_\pm = \frac{1}{2^3} (3b \pm \sqrt{3^2 b^2 + 2^5}). \quad (25)$$

If $v(y_+) < 0$ and $v(y_-) < 0$, four real roots exist, while no real roots for $v(y_+) > 0$ and $v(y_-) > 0$. In the case of $D_4 > 0$, the former condition is equivalent to $v(y_+) + v(y_-) < 0$, which is solved as

$$b^2 > b_x^2 \equiv \frac{2^3}{3} (-1 + 3^{-1/2} \sqrt{1 + 2^3 e}). \quad (26)$$

The term b_x^2 is positive if and only if $e > 1/4$. For $e > 1/4$, one can show $b_x^2 > b_+^2$. If $e > 1/4$, we thus find no images for $b^2 < b_+^2$ and two for $b^2 > b_+^2$, while for $e < 1/4$, four images exist if $b^2 < b_+^2$, and two images if $b^2 > b_+^2$.

We consider the case (b), whose condition is rewritten as

$$f + 4g \cos^2 \phi = g. \quad (27)$$

By substituting this into the first line of Eq. (11), we obtain $a = -2g \cos \phi$. Because of $g \neq 0$, we find

$$\cos \phi = \frac{ar^3}{2e}. \quad (28)$$

Substitution of this into Eq. (27) gives us a cubic equation for r^2 as

$$a^2 r^6 - er^4 + er^2 - e^2 = 0. \quad (29)$$

Because of the symmetry with respect to x-axis, images may appear at $(r \cos \phi, \pm r \sqrt{1 - \cos^2 \phi})$, where r is a solution of Eq. (29) and $\cos \phi$ is obtained by substituting the solution for r into Eq. (28).

Here, we should note a constraint on r , which comes from Eq. (28) for $|\cos \phi| \leq 1$. The constraint is expressed as

$$r \leq \left| \frac{2e}{a} \right|^{1/3}. \quad (30)$$

One can investigate the number of off-axis images according to Eqs. (29) and (30). The detailed discussion is given in the Appendix A. It shows that the maximum number of off-axis images is four if $0 < e < 1/4$, six if $1/4 < e < 1/3$, and two if $e > 1/3$. Similar results in a case of $a = 0$ and $b \neq 0$ are given in the Appendix B.

2.3 Off-axis sources

Here, let us consider off-axis sources, $a \neq 0$ and $b \neq 0$. Then, Eq. (11) implies $\sin \phi \neq 0$ and $\cos \phi \neq 0$, which are equivalent to $\sin 2\phi \neq 0$. By using an inverse matrix, which always exists if $\sin 2\phi \neq 0$, Eq. (11) is rewritten as

$$\begin{pmatrix} f \\ g \end{pmatrix} = \frac{1}{\sin 2\phi} \begin{pmatrix} \sin 3\phi & -\cos 3\phi \\ -\sin \phi & \cos \phi \end{pmatrix} \begin{pmatrix} a \\ b \end{pmatrix} \equiv \begin{pmatrix} F \\ G \end{pmatrix}. \quad (31)$$

Thus r -dependent parts are separated from ϕ -dependent ones. A key is the first line of Eq. (31), which is re-expressed as $r^2 = Fr + 1$. By using this recursively, we obtain $r^3 = (F^2 + 1)r + F$. Substituting this into r^3 in the left hand side of the second line of Eq. (31), we obtain

$$r = -\frac{FG + e}{G(F^2 + 1)}, \quad (32)$$

whose right-hand side depends only on ϕ . This equation implies that G does not vanish for $e \neq 0$ because r is finite. We should note that r cannot be expressed as a function only of $\cot \phi$ but also of $\cos \phi$.

Now, we rewrite F and G as

$$F = \frac{F_0}{2(1 + u^2) \cos \phi}, \quad (33)$$

$$G = \frac{bu - a}{2 \cos \phi}, \quad (34)$$

where

$$u = \cot \phi, \quad (35)$$

$$F_0 = a(3u^2 - 1) - bu(u^2 - 3). \quad (36)$$

Thus, by using Eqs. (32), (33) and (34), we can express (x, y) as a function only of u ,

$$x = -\left(\frac{F_0}{2(1 + u^2)} + \frac{2eu^2}{(bu - a)(1 + u^2)} \right) \times \left(\frac{F_0^2}{4u^2(1 + u^2)} + 1 \right)^{-1}, \quad (37)$$

$$y = -\left(\frac{F_0}{2u(1 + u^2)} + \frac{2eu}{(bu - a)(1 + u^2)} \right) \times \left(\frac{F_0^2}{4u^2(1 + u^2)} + 1 \right)^{-1}. \quad (38)$$

This fact implies that there must exist a master equation determining u . Substituting Eq. (32) into r in the first line of Eq. (31), we obtain a tenth-order equation for $u = \cot \phi$

$$\sum_{k=0}^{10} c_k u^k = 0, \quad (39)$$

where each coefficient is a polynomial in a , b and e as

$$c_{10} = b^4 e, \quad (40)$$

$$c_9 = -10ab^3 e, \quad (41)$$

$$c_8 = 4b^2 + 3b^2 e(4 + 12a^2 - 3b^2), \quad (42)$$

$$c_7 = -8ab - 6abe(8 + 9a^2 - 11b^2), \quad (43)$$

$$c_6 = 4a^2 + 8b^2 + 3e(12a^2 + 9a^4 - 8b^2 - 52a^2 b^2 + 9b^4) - 16e^2, \quad (44)$$

$$c_5 = -16ab + 126abe(a^2 - b^2), \quad (45)$$

$$c_4 = 8a^2 + 4b^2 + 3e(8a^2 - 9a^4 - 12b^2 + 52a^2 b^2 - 9b^4) - 16e^2, \quad (46)$$

$$c_3 = -8ab + 6abe(8 - 11a^2 + 9b^2), \quad (47)$$

$$c_2 = 4a^2 - 3a^2 e(4 - 3a^2 + 12b^2), \quad (48)$$

$$c_1 = 10a^3 b e, \quad (49)$$

$$c_0 = -a^4 e. \quad (50)$$

As seen from Eq. (39), $u = \cot \phi$ neither vanishes nor diverges because $c_{10} \neq 0$ and $c_0 \neq 0$ for a , b and $e \neq 0$. The number of images is constant unless a source crosses the caustics. Therefore, the maximum number of real solutions for Eq. (39) is eight, which equals that for an on-axis source as shown in the preceding subsection. One can see also that there is $c_i \leftrightarrow c_{10-i}$ correspondence with $a \leftrightarrow b$ and $e \leftrightarrow -e$ transformation. This is taken as a justification for the statement regarding the relation between $(a = 0, b \neq 0)$ and $(a \neq 0, b = 0)$.

3 DISCRIMINANT AND CAUSTICS

As well-known in algebra, a discriminant for a real polynomial tells us where the number of real roots changes (for instance, van der Waerden 1966). A discriminant for Eq. (39) is obtained for instance by using Mathematica (Wolfram 2000) as

$$D_{10} = 2^{42} a^{12} b^{12} e^6 W^2 K, \quad (51)$$

where

$$W = (a^2 + b^2)^2 + (a^2 + b^2)^3 - 2e(a^2 - b^2)$$

$$+e^2[1 - (a^2 + b^2) + 3(a^2 + b^2)^2] - e^4[2 - 3(a^2 + b^2)] + e^6, \quad (52)$$

and K is a lengthy polynomial of 494 terms as

$$K = 2^2 3^{16} a^{22} e^5 (2 + 18e + 27b^2 e) + \dots \quad (53)$$

This discriminant D_{10} gives us a condition for changes in the number of real roots for Eq. (39), corresponding to changes in the number of images.

It should be noted that W never vanishes as shown below, which means that r is uniquely determined by Eq. (32). This is in contrast to a case of a binary gravitational lens, for which a squared term such as W^2 can vanish so that a function of r can take a form of “0/0” for particular cases (Asada et al. 2002). By paying attention to an asymmetric term proportional to $a^2 - b^2$ in Eq. (52), we rewrite W as

$$W = (a^2 + b^2 - e + e^2)^2 [a^2 + b^2 + (1 + e)^2] + 4b^2 e, \quad (54)$$

which shows that W is always positive for $b \neq 0$ and $e > 0$. The caustics are thus expressed simply as $K = 0$.

4 CRITICAL CURVES

In the preceding section, the explicit expression for the caustics has been obtained. If we map the expression onto the lens plane by the lens equation, we can obtain the corresponding expression for the critical curves. In practice, however, it is a quite difficult task. Hence, let us study the critical curves in a different way. By a straightforward calculation of the vanishing Jacobian of the lens mapping by Eq. (11),

$$\frac{\partial(a, b)}{\partial(x, y)} = \frac{1}{r} \frac{\partial(a, b)}{\partial(r, \phi)} = 0, \quad (55)$$

we obtain a simple expression for the critical curves as

$$r^8 = r^4 + 9e^2 + 6er^2 \cos 2\phi. \quad (56)$$

This curve is classified topologically into two as follows. Because of $|\cos 2\phi| \leq 1$, Eq. (56) gives a constraint on r

$$|r^8 - r^4 - 9e^2| \leq 6er^2, \quad (57)$$

which is equivalent to

$$r^4 \leq |r^2 + 3e|, \quad (58)$$

and

$$r^4 \geq |r^2 - 3e|, \quad (59)$$

where we used $r^4 \geq 0$. By solving carefully Eqs. (58) and (59), we find for $e \geq 1/12$

$$\frac{-1 + \sqrt{1 + 12e}}{2} \leq r^2 \leq \frac{1 + \sqrt{1 + 12e}}{2}, \quad (60)$$

and for $e < 1/12$,

$$\frac{-1 + \sqrt{1 + 12e}}{2} \leq r^2 \leq \frac{1 - \sqrt{1 - 12e}}{2}, \quad (61)$$

or

$$\frac{1 + \sqrt{1 - 12e}}{2} \leq r^2 \leq \frac{1 + \sqrt{1 + 12e}}{2}. \quad (62)$$

This implies a topological feature of the critical curves: The curves are simply connected if $e \geq 1/12$, or otherwise they are not.

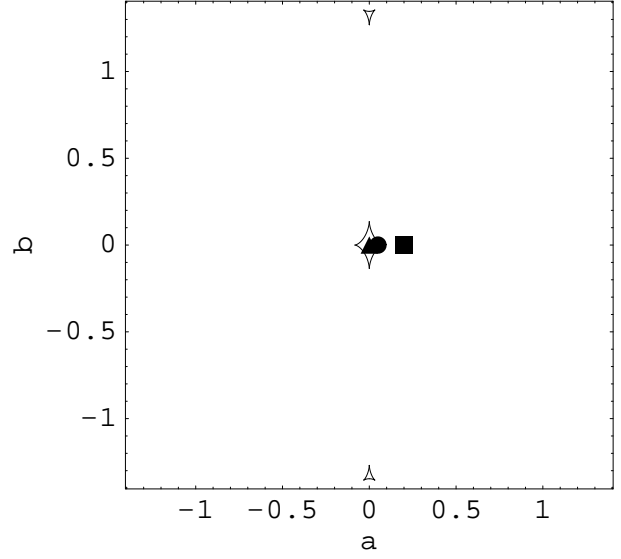


Figure 1. Caustics for a lens with quadrupole moment $e = 0.05$. Sources are located at $(0, 0)$, $(0.05, 0)$ and $(0.2, 0)$, denoted by the triangle, filled disk and square, respectively.

When Eq. (56) is treated as a ϕ -parameter representation of the critical curves, we must solve it as a fourth-order equation for r^2 , so that r^2 can be multi-valued. As a consequence of $r \geq 0$, furthermore, some domains of the parameter $\phi \in [0, 2\pi)$ can be excluded. It seems thus much simpler to consider Eq. (56) as a representation with a parameter r which is allowed by Eq. (60) for $e \geq 1/12$ or by Eqs. (61) and (62) for $e < 1/12$. The representation becomes

$$(x, y) = (\pm r \sqrt{\frac{1+h}{2}}, \pm r \sqrt{\frac{1-h}{2}}), \quad (63)$$

where we defined

$$h = \frac{r^8 - r^4 - 9e^2}{6er^2}. \quad (64)$$

In addition, substitution of this parametric representation into the right-hand side of Eq. (11) gives us a representation of the caustics with the same parameter as

$$a(r) = \pm [f + g(2h - 1)] \sqrt{\frac{1+h}{2}}, \quad (65)$$

$$b(r) = \pm [f + g(2h + 1)] \sqrt{\frac{1-h}{2}}. \quad (66)$$

As illustrations, the caustics and critical curves for $e = 0.05 < 1/12$ are given by Figs. 1 and 2, respectively. Actually, there are three closed loops of critical curves. A case of $e = 0.1 > 1/12$ is shown by Figs. 3 and 4.

5 CONCLUSION

We have re-examined the lens equation for a gravitational lens due to a deformed star modeled by using quadrupole moment. First, we reduce the lens equation to a single real tenth-order polynomial. Consequently, an analytic expression for the caustics is given by Eq. (53) as $K = 0$, though it is too lengthy to handle. The critical curves are simply

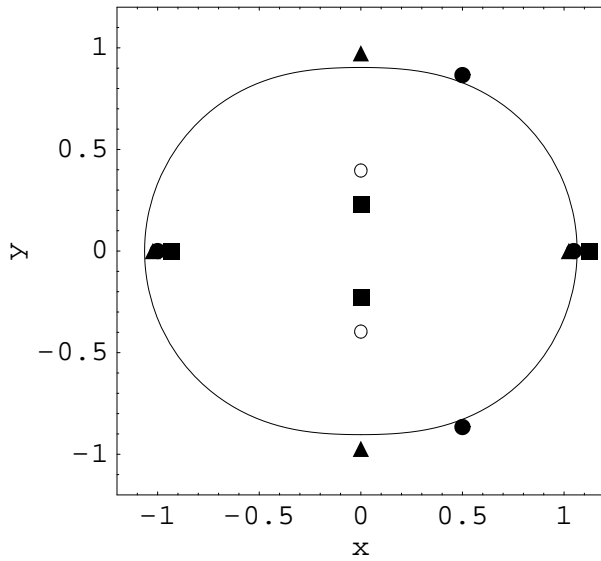


Figure 2. Critical curves for a lens with quadrupole moment $e = 0.05$. The images correspond to the sources in Fig. 1. Triangles, Filled disks and squares are overlapped around $(0, \pm 0.2)$.

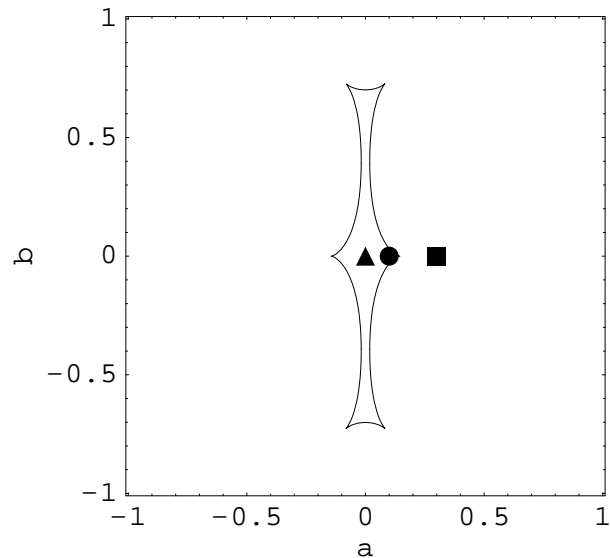


Figure 3. Caustics for a lens with quadrupole moment $e = 0.1$. Sources are located at $(0, 0)$, $(0.1, 0)$ and $(0.3, 0)$, denoted by the triangle, filled disk and square, respectively.

expressed as Eq. (56) or Eq. (63). The parametric representation of the caustics is given by Eqs. (65) and (66). Hence, the present result must be helpful for understanding the gravitational lensing due to a deformed star. In particular, it gives a nice approximation to a lensing study based on a realistic numerical simulation of a compact object.

For instance, the image position is unstable for a source close to the caustics, so that careful numerical computations are needed. The present approach will make it easy to study such a case. This is a future subject.

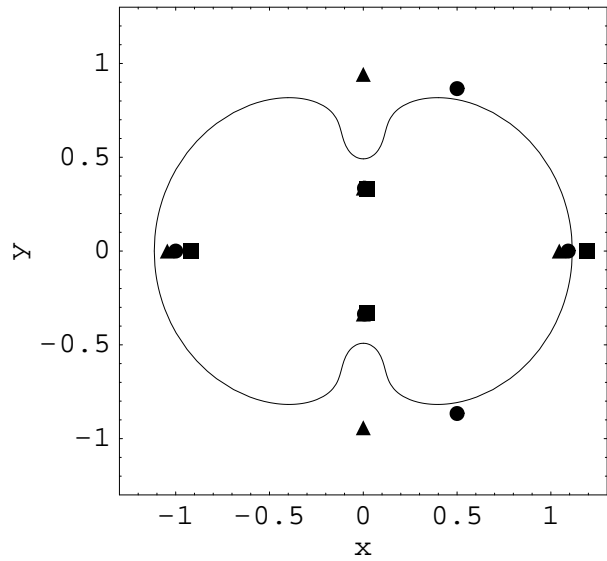


Figure 4. Critical curves for a lens with quadrupole moment $e = 0.1$. The images correspond to the sources in Fig. 3. Triangles, Filled disks and squares are overlapped around $(0, \pm 0.3)$.

ACKNOWLEDGMENTS

The author would like to thank the anonymous referee for invaluable comments especially about the classification of the number of images for on-axis sources. He would like to thank E. Berti for fruitful conversations. He would like to thank L. Blanchet for hospitality at the Institute for Astrophysics at Paris. This work was supported by a fellowship for visiting scholars from the Ministry of Education of Japan.

REFERENCES

- Asada H., & Kasai M., 2000 *Prog. Theor. Phys.*, 104, 95
- Asada H., 2002 *A&A*, 390, L11
- Asada H., Kasai T., Kasai M., 2002 *Prog. Theor. Phys.*, 108, 1031
- Asada H., Hamana T., Kasai M., 2003 *A&A*, 397, 825
- Asada H., Kasai T., Kasai M., 2004 *Prog. Theor. Phys.*, 112, 241
- Chandrasekhar S., 1987 *Ellipsoidal Figures of Equilibrium* (New York: Dover)
- Dominik M., 1999 *A&A*, 349, 108
- Epstein R., Shapiro I. I., 1980 *Phys. Rev. D*, 22, 2947
- Kovner I., 1987 *ApJ*, 312, 22
- Shapiro S. L., Teukolsky S. A., 1983 *Black Holes, White Dwarfs, and Neutron Stars* (New York: Wiley)
- Schneider P., Ehlers J., Falco E. E., 1992 *Gravitational Lenses* (Springer-Verlag)
- Shibata M., Karino S., Eriguchi Y., 2002 *MNRAS*, 334, L27
- Stergioulas N., Apostolatos T. A., Font J. A., 2004 *MNRAS*, 352, 1089
- van der Waerden B. L., 1966 *Algebra I* (Springer)
- Will, C. M. 1993, *Theory and Experiment in Gravitational Physics* (Cambridge: Cambridge Univ. Press)
- Wolfram S., 2000 *The Mathematica Book, 4th ed.* (Cambridge: University Press)
- Zanotti O., Rezzolla L., 2002 *MNRAS*, 331, 376

Zdunik J. L., Haensel P., Gourgoulhon E., Bejger M., 2004
A&A, 416, 1013

APPENDIX A: CLASSIFICATIONS OF OFF-AXIS IMAGES I.

Let us investigate the number of off-axis images according to Eqs. (29) and (30) in a case of $a \neq 0$ and $b = 0$. They are rewritten as

$$g(p) \equiv a^2 p^3 - ep^2 + ep - e^2 = 0, \quad (\text{A1})$$

$$p \leq \left| \frac{2e}{a} \right|^{2/3} \equiv p_0, \quad (\text{A2})$$

where we defined $p = r^2$. The discriminant of Eq. (A1) is

$$D_3 = -e^3[3^3 ea^4 + (2^2 - 2 \cdot 3^2 e)a^2 - (e - 2^2 e^2)]. \quad (\text{A3})$$

$D_3 = 0$ has two roots as

$$a^2 = A_{\pm}, \quad (\text{A4})$$

where we defined

$$A_{\pm} = \frac{1}{3^3 e} [(3^2 e - 2) \pm 2(1 - 3e)^{3/2}]. \quad (\text{A5})$$

We find $A_- > 0$ if $e > 1/4$, and otherwise $A_- < 0$. We find $g(p_0)$ as

$$g(p_0) = \frac{e^{5/3}}{a^{4/3}} (3e^{1/3} a^{4/3} - 2^{4/3} e^{2/3} + 2^{2/3} a^{2/3}). \quad (\text{A6})$$

The condition that $g(p_0) > 0$ is

$$a^2 > A_0 \equiv \frac{2}{3^3 e} [-(1 + 3^2 e) + (1 + 3e)\sqrt{1 + 2^2 3e}], \quad (\text{A7})$$

where we used the positivity of a^2 .

In order to analyse the number of the valid solutions satisfying Eq. (A2), one needs to investigate the signature not only of $g(p_0)$ but also of $g'(p_0)$. In a case of $g(p_0) < 0$ and $g'(p_0) > 0$, for instance, one can show that there exists a root $p > p_0$, which corresponds to an unphysical solution r violating the condition (30). The condition that $g'(p_0) < 0$ is

$$a^2 < A_1 \equiv \frac{1}{2^5 3^3 e} [-(1 + 2^3 3^2 e) + (1 + 2^3 3e)\sqrt{1 + 2^5 3e}], \quad (\text{A8})$$

where we used the positivity of a^2 .

The number of the valid solutions are found by figuring out the relative order among a^2 , A_{\pm} , A_0 and A_1 , which depends on the value of e . Straightforward but tedious computations give the following result.

(1) $0 < e < \frac{1}{4}$

(1a) $A_- < 0 < a^2 < A_0 < A_+ < A_1$

There are three positive roots. Only two of them are valid and thus four off-axis images exist.

(1b) $A_- < A_0 < a^2 < A_+ < A_1$

There are three positive roots. Only one of them is valid and thus two off-axis images exist.

(1c) $A_- < A_0 < A_+ < a^2 < A_1$

There is only one positive root, which is still valid. Thus two off-axis images exist.

(1d) $A_- < A_0 < A_+ < A_1 < a^2$

There is only one positive root, which is still valid. Thus two off-axis images exist.

(2) $\frac{1}{4} < e < \frac{8}{25}$

The relative order between A_- and A_1 is not unique in this case.

(2a) $0 < a^2 < A_-, A_1 < A_0 < A_+$

There is only one positive root, which is not valid. Thus no off-axis images exist.

(2b) $0 < A_- < a^2 < A_1 < A_0 < A_+$

There are three positive roots. Only two of them are valid and thus four off-axis images exist.

(2c) $0 < A_1 < a^2 < A_- < A_0 < A_+$

There is only one root, which is not valid. Thus no off-axis images exist.

(2d) $0 < A_-, A_1 < a^2 < A_0 < A_+$

There are three positive roots. Only two of them are valid and thus four off-axis images exist.

(2e) $0 < A_-, A_1 < A_0 < a^2 < A_+$

There are three positive roots, all of which are still valid. Thus six off-axis images exist.

(2f) $0 < A_-, A_1 < A_0 < A_+ < a^2$

There are only one positive root, which is still valid. Thus two off-axis images exist.

(3) $\frac{8}{25} < e < \frac{1}{3}$

(3a) $0 < a^2 < A_1 < A_0 < A_- < A_+$

There is only one positive root, which is not valid. Thus no off-axis images exist.

(3b) $0 < A_1 < a^2 < A_0 < A_- < A_+$

There is only one positive root, which is not valid. Thus no off-axis images exist.

(3c) $0 < A_1 < A_0 < a^2 < A_- < A_+$

There is only one positive root, which is still valid. Thus two off-axis images exist.

(3d) $0 < A_1 < A_0 < A_- < a^2 < A_+$

There are three positive roots, all of which are still valid. Thus six off-axis images exist.

(3e) $0 < A_1 < A_0 < A_- < A_+ < a^2$

There is only one positive root, which is still valid. Thus two off-axis images exist.

(4) $\frac{1}{3} < e$

(4a) $0 < a^2 < A_1 < A_0$

There is only one positive root, which is not valid. Thus no off-axis images exist.

(4b) $0 < A_1 < a^2 < A_0$

There is only one positive root, which is not valid. Thus no off-axis images exist.

(4c) $0 < A_1 < A_0 < a^2$

There is only one positive root, which is still valid. Thus two off-axis images exist.

APPENDIX B: CLASSIFICATIONS OF OFF-AXIS IMAGES II.

We classify the number of off-axis images in a case of $a = 0$ and $b \neq 0$. The transformation of $a \leftrightarrow b$ and $e \leftrightarrow -e$ changes Eq. (29) as

$$b^2 r^6 + er^4 - er^2 - e^2 = 0. \quad (\text{B1})$$

The constraint by Eq. (30) is also transformed into

$$r \leq \left| \frac{2e}{b} \right|^{1/3}. \quad (\text{B2})$$

Let us investigate the number of off-axis images according to Eqs. (B1) and (B2) in a case of $a = 0$ and $b \neq 0$. They are rewritten as

$$h(q) \equiv b^2 q^3 + eq^2 - eq - e^2 = 0, \quad (\text{B3})$$

$$q \leq \left| \frac{2e}{b} \right|^{2/3} \equiv q_0, \quad (\text{B4})$$

where we defined $q = r^2$.

One can show that the positive root is always only one because $h(0) < 0$ and $h'(0) < 0$. This situation is much simpler than that of $a \neq 0$ and $b = 0$. Namely, one can show that the valid solution is still one if $h(q_0) > 0$, while we have no valid solution if $h(q_0) < 0$. We find $h(q_0) > 0$ always holds if $e > 1/12$. If $e < 1/12$, $h(q_0) > 0$ is equivalent to $b^2 < B_-$ or $b^2 > B_+$, where we defined

$$B_{\pm} = \frac{2}{3^3 e} [(1 - 3^2 e) \pm (1 - 3e) \sqrt{1 - 2^2 \cdot 3e}]. \quad (\text{B5})$$

As a result, the number of the off-axis images is classified as follows.

$$(1) \ e < \frac{1}{12}$$

$$(1a) \ 0 < b^2 < B_-$$

There is only one positive root, which is still valid. Thus two off-axis images exist.

$$(1b) \ B_- < b^2 < B_+$$

There is only one positive root, which is not valid. Thus no off-axis images exist.

$$(1c) \ B_+ < b^2$$

There is only one positive root, which is still valid. Thus two off-axis images exist.

$$(2) \ e > \frac{1}{12}$$

$$(2a) \ 0 < b^2$$

There is only one positive root, which is still valid. Thus two off-axis images exist.

This paper has been typeset from a $\text{\TeX}/\text{\LaTeX}$ file prepared by the author.